Supplementary Information

Rational Design of Ion-Conducting and Interface-Optimized Acrylate-Based Network Binder Employed in Silicon/Graphite Anode for Li-ion Battery

Renjie Zhou [a,b], *Xuefeng Gui* [a,b,c,d,e,*], *Ziyang Gong* [a,b], *Jiwen Hu* [a,b,c,d,e,**], *Yafang Han* [a,b], *Xiaohua Cui* [a,b], *Yang Liu* [a,b], *Weixin Li* [a,b]

[a] *Guangzhou Institute of Chemistry, Chinese Academy of Sciences, Guangzhou 510650, People's Republic of China*

[b] *University of the Chinese Academy of Sciences, Beijing 100049, People's Republic of China*

[c] *CAS Engineering Laboratory for Special Fine Chemicals, Guangzhou 510650, People's s Republic of China*

[d] *CASH GCC Shaoguan Research Institute of Advanced Materials, Nanxiong 512400, China*

[e] *CASH GCC (Nanxiong) Research Institute of Advanced Materials Co., Ltd., Nanxiong 512400, People's Republic of China*

* Corresponding author. Email address: guixf@gic.ac.cn (Xuefeng Gui)

** Corresponding author. Email address: hjw@gic.ac.cn (Jiwen Hu)

Materials

In this study, the monomers acrylic acid (AA), butyl acrylate (BA), methyl methacrylate (MMA), hydroxyethyl acrylate (HEA) used for polymerization were purchased from Aladdin Biochemical Technology Co., LTD (Shanghai, China). Before use, all monomers were purified by vacuum distillation. Sodium carboxymethyl cellulose (CMC-Na, DS = 0.9), polyacrylic acid (PAA, M_W = 450000) and ammonium persulfate (APS) were all obtained from Shanghai Macklin Biochemical Co., LTD (Shanghai, China). Reactive emulsifiers 1-allyloxy-3-(4-nonylphenol)-2-propanol polyoxyethylene (10) ether ammonium sulfate (DN-86) and 1-allyloxy-3-(4-nonylphenol)-2-propanol polyoxyethylene (10) ether (AS-10) and were provided by Hanke Chemical Technology Co., LTD (Nanxiong, China).

Characterizations

Infrared spectroscopy (IR) was conducted using the Fisher Scientific Nicolet iS20 spectrometer equipped with the attenuated total reflectance (ATR) accessory over the range of 400 - 4000 cm^{-1}. Differential scanning calorimetry (DSC) measurements were carried out on the DSC25 instrument (TA Instruments, United States) in the temperature range of -50 to 200 °C under a nitrogen atmosphere, with a heating rate of 10 °C min^{-1}. Thermogravimetric analysis (TGA) was performed using the TG 209 F3 synchronous thermal analyzer (Netzsch, Germany), and the TGA characterization was conducted under a nitrogen atmosphere in the temperature range of 30 - 800 °C, with a heating rate of 10 °C min^{-1}. Scanning electron microscopy (SEM) images were obtained using

a MIRA LMS scanning electron microscope (TESCAN, Czechia). The 180° peeling force test was performed on an Instron 5965 electronic universal testing machine (Instron, United States) using 3M adhesive tape (2 cm in width) affixed to the electrode surface, at a constant peeling rate of 10 mm min^{-1}. Each group of samples was tested three times to ensure the accuracy and reproducibility of the results. The same instrument was also used for the vertical tensile test. For this test, each binder sample was cut into dumbbell-shaped strips with dimensions of 20 mm × 4 mm × 2 mm, and the measurements were conducted in triplicate at a constant displacement rate of 10 mm min^{-1}.

The electrolyte absorption rates of the binders were calculated by the following equation [1]:

$$\text{Swelling ratio} = \frac{W - W_0}{W_0} \times 100\%$$

where W(mg) and W_0(mg) represent the masses of the wet and dry samples, respectively. Each set of samples was tested three times, and the reported results are the average values calculated from these repeated measurements.

Electrochemical Tests

The CR2032 button-type batteries were assembled in an argon-filled glove box. Half-cells were installed using lithium sheets as the counter electrodes. Full cells were prepared using LFP as the cathode (Φ12 mm) with an N/P ratio guaranteed to be 1.1. The electrolyte (supplied by Canrd) was comprised of 1.0 M $LiPF_6$, which was dissolved in a mixture of methyl ethyl carbonate, ethylene carbonate, and diethyl

carbonate containing 5 vol% fluoroethylene carbonate (EMC/EC/DEC, 1:1:1 by volume). Si/C materials (1C = 850 mAh/g) and diaphragms (Celgard 2500) were supplied by Canrd. The operating voltage range of the cyclic voltammetry (CV) curve was 0.01-3 V. The alternating current (AC) impedance spectroscopy tests were measured on a CHI600e electrochemical workstation within the frequency range of 0.01-100 kHz. The galvanostatic charge/discharge tests were conducted on the LAND battery test system (CT3002A, Wuhan, China) with a voltage range of 0.01 - 1.5 V for half-cell and 2.5 - 4V for full cell.

Computational details of density functional theory

Density functional theory (DFT) calculations were carried out using the Gaussian 16 software package. All calculations employed the B3LYP function with D3BJ dispersion correction. Geometry optimizations and frequency analyses for the atoms were performed using the 6-31G basis set, while single-point energy calculations were conducted at the B3LYP-D3BJ/6-311G (d, p) level [2-4]. The binding energy (E_b) between molecule A and Li^+ was calculated based on the following equation:

$$E_b = E_{(A + Li^+)} - (E_A + E_{Li^+})$$

Here, $E_{(A + Li^+)}$ is the total energy of the complex formed by molecule A and Li^+. E_A and E_{Li^+} denote the energies of isolated molecule A and isolated Li^+, respectively. The frontier molecular orbitals (HOMO and LUMO) were constructed and visualized using the Multiwfn wavefunction analyzer in combination with the Visual Molecular Dynamics (VMD) software package [5].

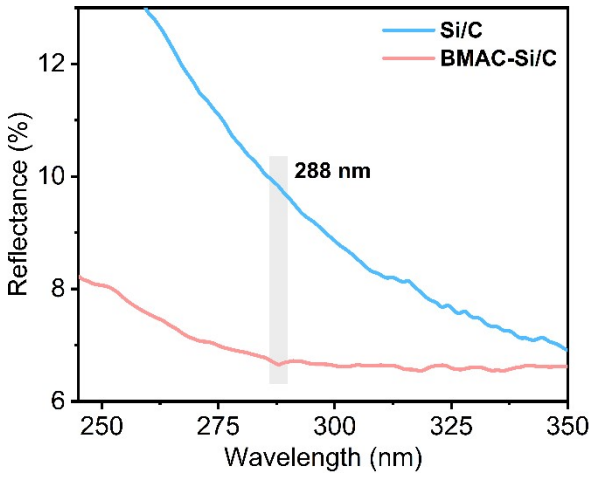

Figure S1. UV-vis reflectance spectra of Si/C materials before and after introducing BMAC binder. It is clearly visible that the Si/C materials after the introduction of BMAC binder exhibits the characteristic reflection valley at 288 nm caused by π-π stacking of phenyl groups.

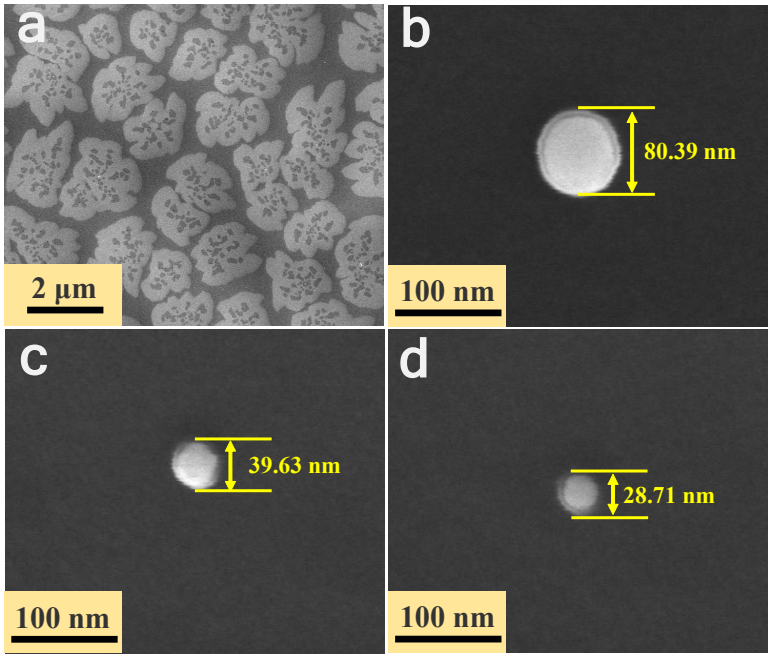

Figure S2. SEM images of BMA emulsion after freeze-drying. a) Intersecting structure of soft and hard chain segments. b)-d) Captured intact latex particles.

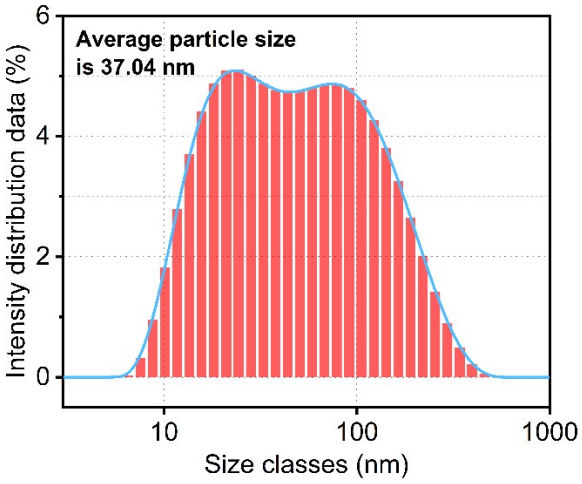

Figure S3. a) Particle size distribution and b) zeta potential dispersed in deionized water of BMA emulsion

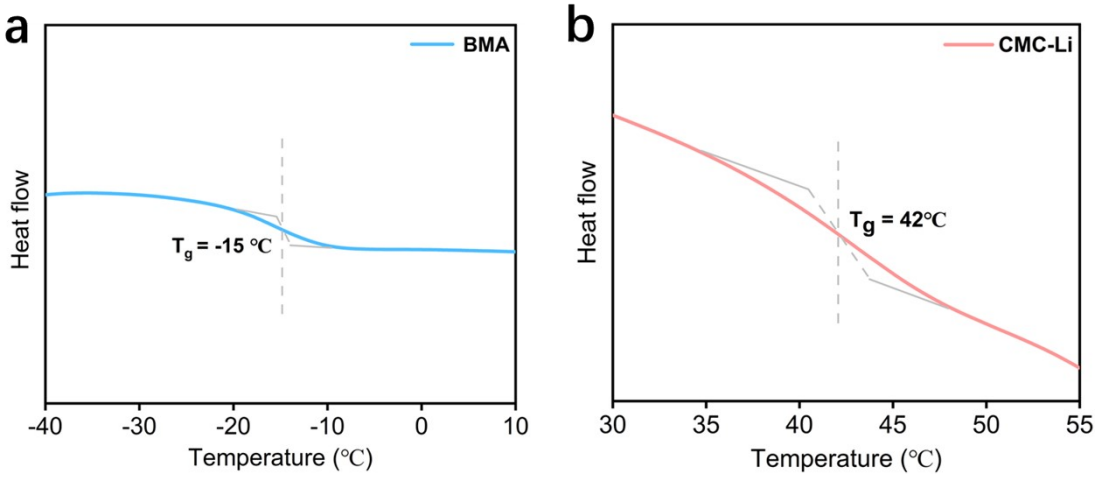

Figure S4. DSC curves for a) BMA and b) CMC-Li.

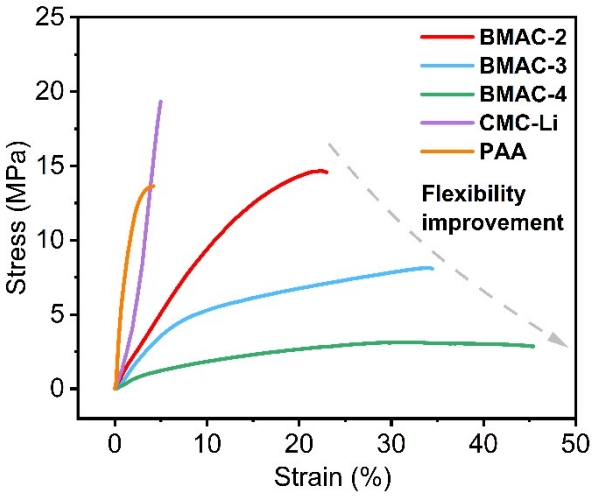

Figure S5. Stress-strain curves obtained from tensile strength tests of BMAC-2, BMAC-3, BMAC-4, CMC-Li, and PAA binders.

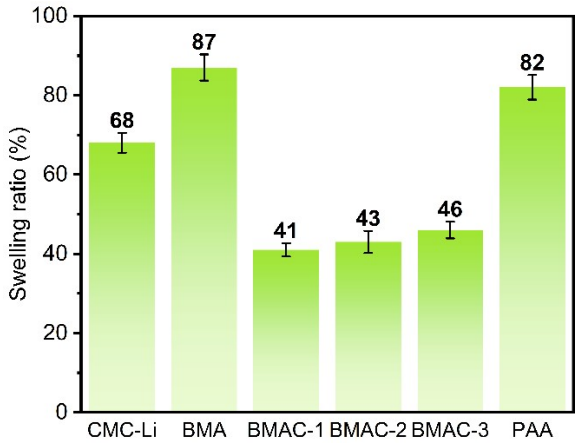

Figure S6. Electrolyte uptake of CMC-Li, BMA, BMAC, and PAA binders after 6 h.

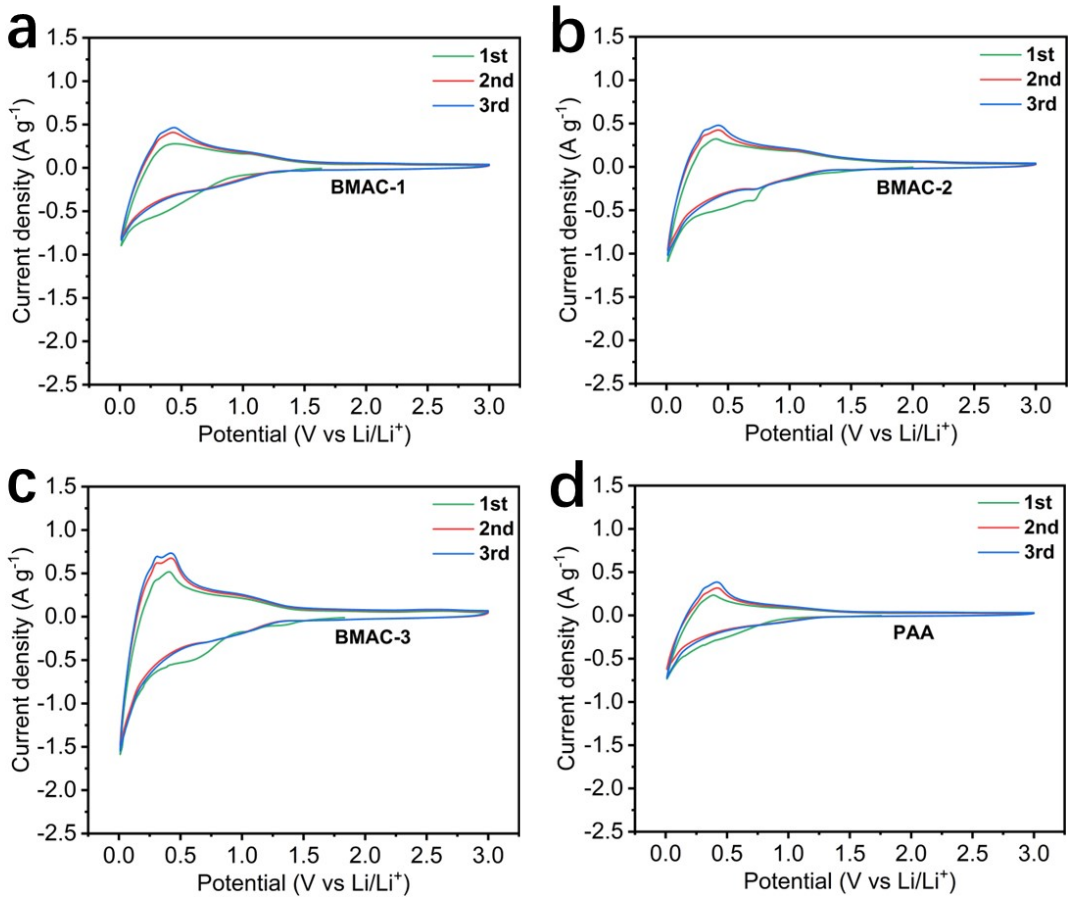

Figure S7. CV curves of the Si/C anodes prepared by BMAC-1, BMAC-2, BMAC-3, and PAA.

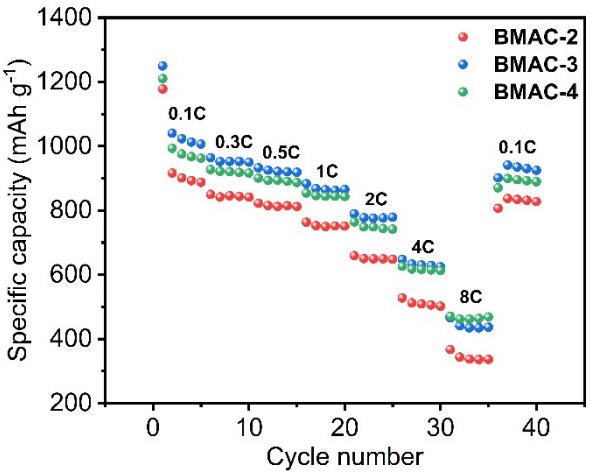

Figure S8. C-rate performance of Si/C/BMAC-2, Si/C/BMAC-3, and Si/C/BMAC-4 in the 0.1-8C current density interval.

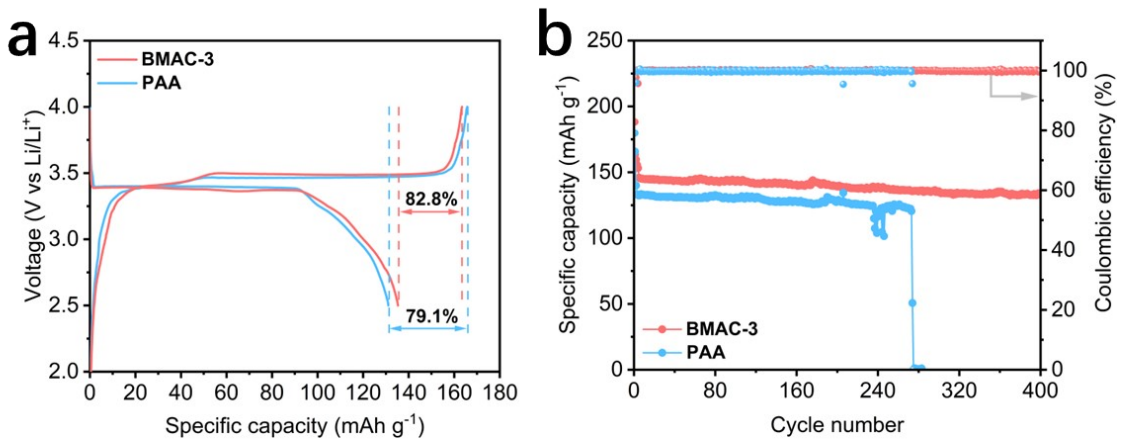

Figure S9. The electrochemical performance of the full cell with BMAC and PAA anodes. (a) Initial charge-discharge curves of Si/C/BMAC and Si/C/PAA full cells at 0.1C. (b) The long-term cycling stability and coulombic efficiency of the Si/C/BMAC and Si/C/PAA full cells at 0.5 C

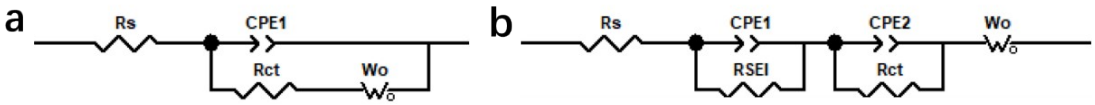

Figure S10. Equivalent circuit models corresponding to the Nyquist curves recorded. a) before and b) after cycling of Si/C anodes.

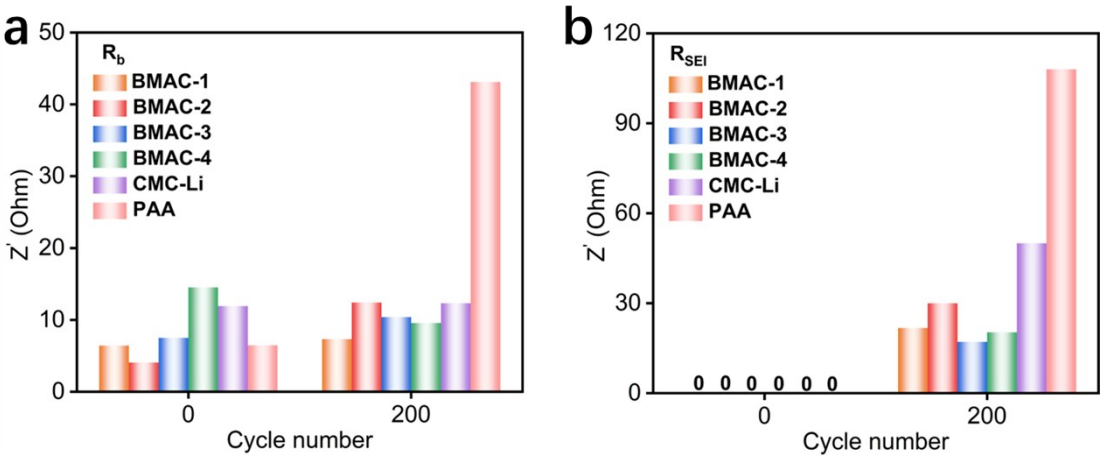

Figure S11. The trend comparisons for a) R_b and b) R_{SEI} of Si/C/BMAC-1, Si/C/BMAC-2, Si/C/BMAC-3, Si/C/BMAC-4, Si/C/CMC-Li, and Si/C/PAA are analyzed and shown in the corresponding bar graphs

Table S1. Impedance parameters of Si/C electrodes prepared with different binders. These values were measured before cycling.

Samples	R_b	R_{SEI}	R_{ct}
BMAC-1	6.40	0	70.05
BMAC-2	4.06	0	70.89
BMAC-3	7.49	0	50.34
BMAC-4	14.52	0	95.77
CMC-Li	11.90	0	148.02
PAA	6.46	0	221.34

Table S2. Impedance parameters of Si/C electrodes prepared with different binders. These parameters were measured after 200 cycles.

Samples	R_b	R_{SEI}	R_{ct}
BMAC-1	7.32	21.73	62.65
BMAC-2	12.40	29.95	55.89
BMAC-3	10.40	17.10	30.08
BMAC-4	9.54	20.30	40.01
CMC-Li	12.30	50.00	68.78
PAA	43.10	108.03	162.43

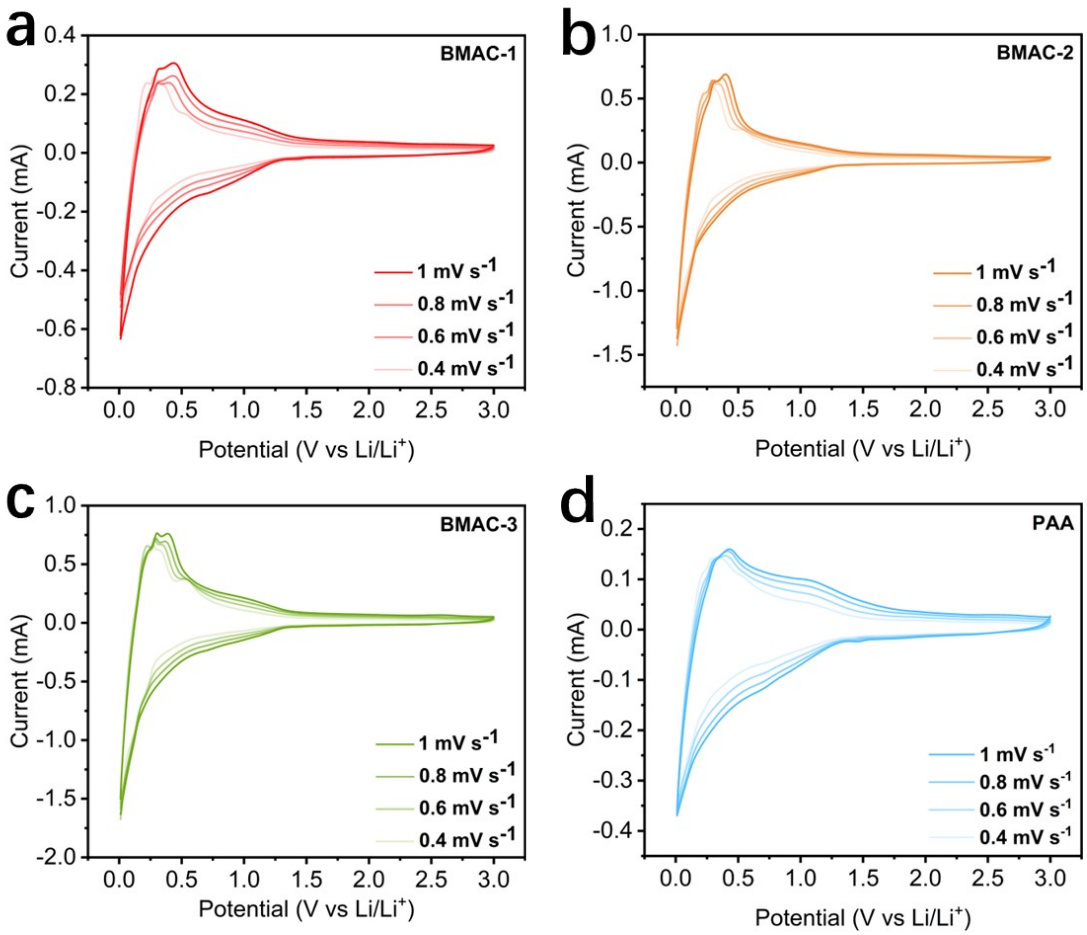

Figure S12. CV curves of a) BMAC-1, b) BMAC-2, c) BMAC-3 and d) PAA at different voltage scan rates.

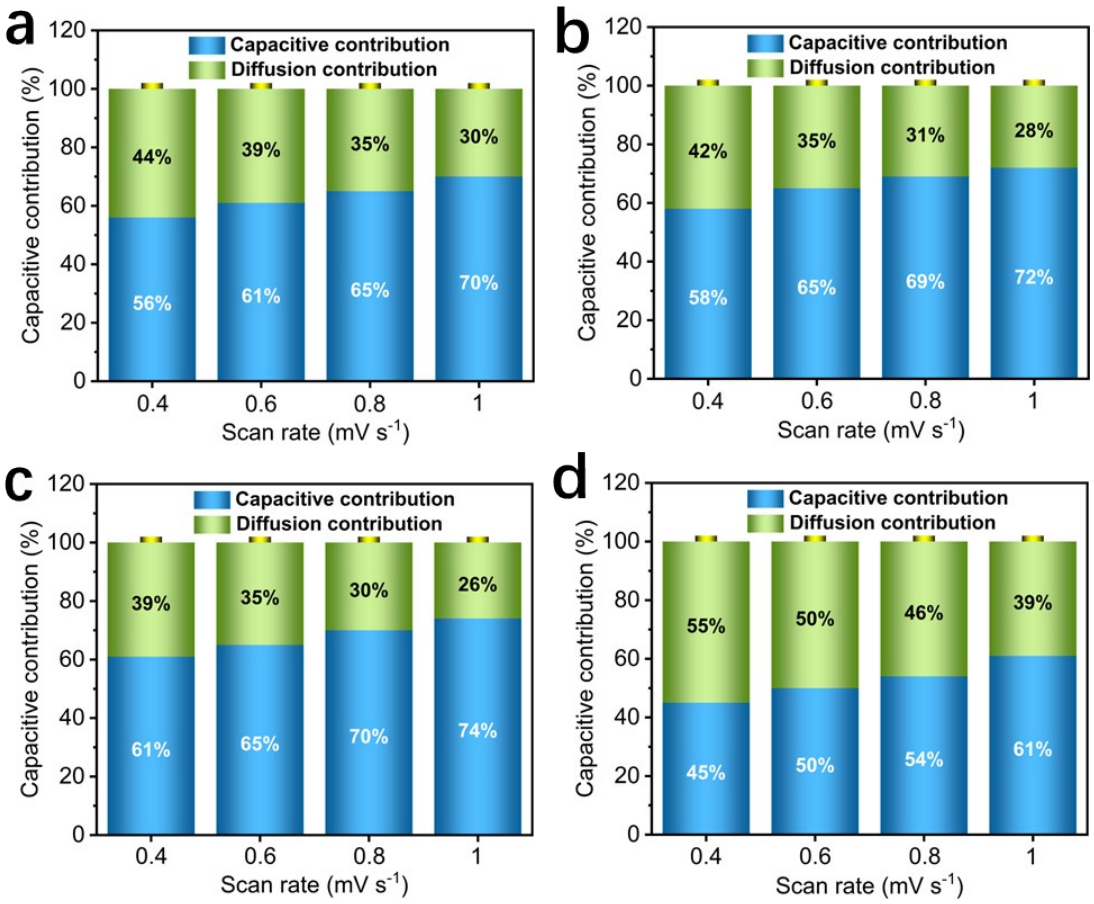

Figure S13. Capacitive control contributions of a) BMAC-1, b) BMAC-2, c) BMAC-3, and d) PAA.

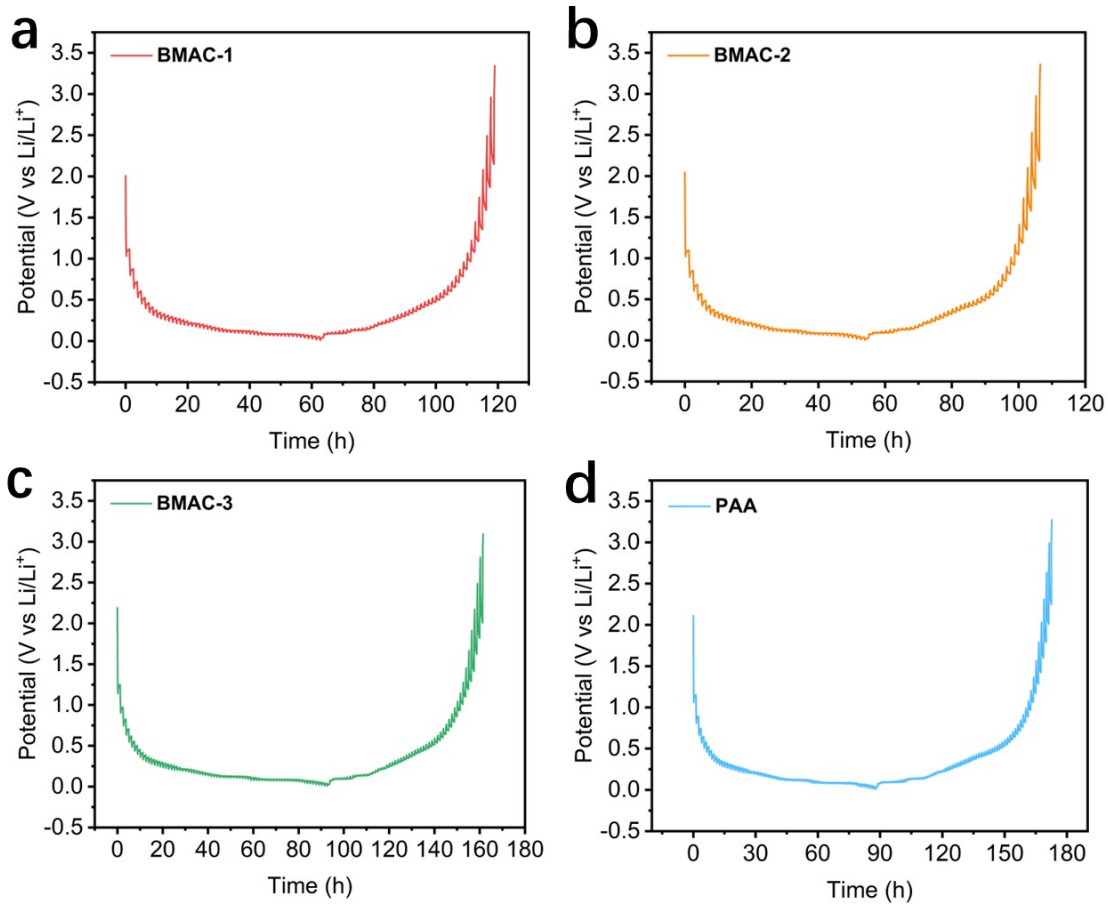

Figure S14. GITT curves of a) BMAC-1, b) BMAC-2, c) BMAC-3, and d) PAA.

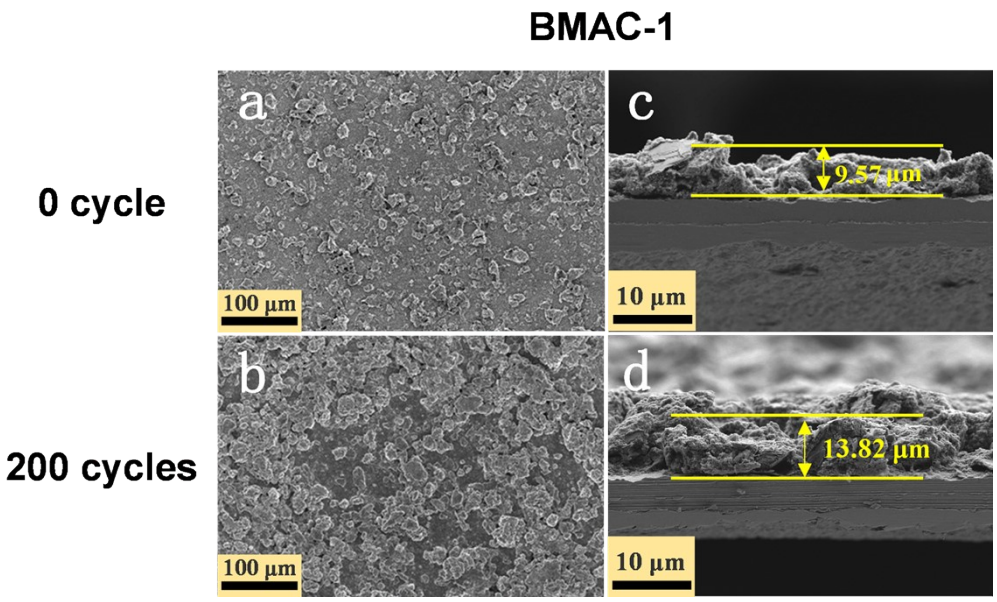

Figure S15. Top-view SEM images showing the morphological evolution of Si/C/BMAC-1 a) before cycling and b) after 200 cycles. Cross-sectional SEM images of the tested anodes c) before cycling and d) after 200 cycles.

Table S3. Performance comparison of each SEI component in lithium-ion battery system [6-8].

	Mechanical property	Electrochemical stability	Electronic insulation
LiF	Good (Mechanically robust)	Good	Good
Li_2CO_3	Bad (Brittle and fragile)	Bad (High reactivity with the electrolyte)	—
$Li_xPO_yF_z$	Bad (Brittle and fragile)	Bad (Prone to decomposition during electrochemical cycling)	—
Li_xSiO_y	Bad (Brittle and fragile)	Bad (Prone to decomposition during electrochemical cycling)	—

Table S4. Summary of the electrochemical performances of various Si/C anodes.

Binder	Theoretical specific capacity (mAh g^{-1})	Loading (mg cm^{-2})	Electrochemical performance
Diglycidyl ether crosslinked carboxymethyl chitosan (CCS-EG)[9]	600	1.5	474 mAh g^{-1} after 400 cycles at 0.5C (88% capacity retention)
			187 mAh g^{-1} at 4C
Acrylate-based ion-conductive network binder (PAMN)[10]	650	1.0-1.2	560 mAh g^{-1} after 400 cycles at 1C (87% capacity retention)
			350 mAh g^{-1} at 4C
Chitosan-based ion-conducting network binder (LiCB)[11]	650	1.1	ICE = 82.18%
			600 mAh g^{-1} after 200 cycles at 1C
			220 mAh g^{-1} at 4C
Acrylic-based triblock copolymer (PSEA)[12]	950	2.3	ICE = 85.10%
			652 mAh g^{-1} after 400 cycles at 0.5C with 82% capacity retention
			450 mAh g^{-1} at 2C
A composite binder of sodium alginate, polyacrylamide gel and polytetrafluoroethylene (PSAP663)[13]	650	0.6-1	427 mAh g^{-1} after 300 cycles at 0.5 A g^{-1}
			238 mAh g^{-1} at 1.2 A g^{-1}
A water-processable multifunctional copolyimide binder (SPI-40)[14]	950	2	ICE = 83.6%
			825.2 mAh g^{-1} after 400 cycles at 0.5 A g^{-1}
			701.6 mAh g^{-1} at 2.0 A g^{-1}
Dual-crosslinked network binder of alginate with polyacrylamide (Alg-g-PAAm)[15]	1200	1.3	ICE = 72.8%
			836 mAh g^{-1} after 100 cycles at 0.1C with 71.6% capacity retention
Fluorine-containing soluble polyimide binder (PI-FN)[16]	650	0.54	270.3 mAh g^{-1} at 5C
			352.4 mAh g^{-1} after 500 cycles with about 50% capacity retention
BMAC (This work)	850	1.2-1.3	ICE = 87.98%
			818.8 mAh g^{-1} after 200 cycles at 1C with 98.6% capacity retention; 419.5 mAh g^{-1} after 800 cycles at 2C with 61.4% capacity retention
			630.3 mAh g^{-1} at 4C; 462.3 mAh g^{-1} at 8C

Table S5. Scalability and practicality of the BMAC binder[17-20].

Scalable preparation process
The BMAC binder is synthesized via emulsion polymerization combined with in-situ thermal crosslinking strategy. Both processes do not rely on special equipment and do not require extreme temperatures or high pressures, which is in line with the conditions for the preparation of industrial polymers, and is promising for scaling up. Specifically, emulsion polymerization, owing to its excellent heat dissipation capability, mild reaction conditions, and the use of water as the continuous phase, has been widely adopted for large-scale polymer manufacturing, ensuring both process safety and environmental friendliness. In addition, the in situ thermal crosslinking strategy eliminates the need for post-treatment or additional crosslinking steps, thereby reducing process complexity and overall fabrication cost. Importantly, thermal crosslinking can be readily integrated into the electrode drying process without requiring extra equipment investment or substantial modifications to existing production lines. Collectively, the combination of emulsion polymerization and in situ thermal crosslinking endows the preparation process of the BMAC binder with high scalability and strong industrial feasibility.
Rational selection of raw materials
The BMAC binder is prepared from acrylate-based monomers and CMC-Li, both of which offer clear advantages in terms of practicality and scalability. Acrylate monomers are widely available and cost-effective, while CMC-Li is a water-soluble, renewable cellulose derivative with a mature synthesis process and controllable cost, providing effective adhesion and contributing to network formation during electrode fabrication. Compared with conventional oil-based PVDF binder, the raw materials used for the synthesis of the BMAC binder are entirely water-soluble and do not involve toxic and volatile organic solvents (e.g., N-methyl-2-pyrrolidone, NMP), thereby eliminating environmental concerns and reducing processing costs. In contrast to commercial anode binders such as PAA and carboxymethyl cellulose-styrene/butadiene rubber (CMC-SBR), the BMAC binder system enables the synergistic optimization of mechanical properties, adhesion performance, and electrochemical functionality through rational regulation of the functional component ratios. This high degree of functional and structural tunability endows the BMAC binder with excellent application adaptability, allowing it to flexibly meet the requirements of different application scenarios. Notably, some reported advanced binder systems rely on multistep synthetic routes, suffer from low reaction yields, and depend on expensive specialty monomers, which to some extent limit their practical applicability. By comparison, the rational design of monomer system and the preparation process in this work effectively circumvents these issues, significantly enhancing the scalability and practicality of the proposed binder system.
Performance benefits for practical viability
The extreme long-term cycling test conducted at 2 C demonstrate that Si/C anode containing BMAC binder exhibits excellent cycling stability, which is expected to extend the service life of batteries in practical applications, reduce electrode replacement frequency, and thereby effectively lower the overall cost. The cell rate tests in the range of 0-8 C reveal that the superior lithium-ion transport capability imparted by the BMAC binder enables the Si/C anode to sustain stable specific capacity output under the high current densities, thus satisfying the requirements of commercial batteries for high-power applications. Compared with Si/C/PAA, the Si/C anode incorporating the BMAC binder exhibits the higher initial coulombic efficiency and superior cycling stability in the LFP full cell, further demonstrating the practical viability of BMAC.

References

1. G. Z. Xu, X. C. Xie, L. Qin, X. J. Hu, D. L. Zhang, J. Xu, D. W. Li, X. W. Ji, Y. Huang, Y. Z. Tu, L. Jiang and D. Y. Wei, *Green Chem.*, 2019, **21**, 6062-6072.
2. S. Grimme, J. Antony, S. Ehrlich and H. Krieg, *J. Chem. Phys.*, 2010, **132**, 19.
3. Harihara.Pc and J. A. Pople, *Theor. Chim. Acta*, 1973, **28**, 213-222.
4. W. J. Hehre, R. Ditchfield and J. A. Pople, *J. Chem. Phys.*, 1972, **56**, 2257-+.
5. T. Lu and F. W. Chen, *J. Comput. Chem.*, 2012, **33**, 580-592.
6. Z. Li, L. Wang, X. D. Huang and X. M. He, *Small*, 2024, **20**, 18.
7. T. Jia, G. Zhong, S. Lu, X. Ren, Y. Lv, N. Li, R. Yin, G. Kang, K. Cai, F. Kang and Y. Cao, *Chem. Eng. J.*, 2023, **454**, 140397.
8. H. Jin, S. Pyo, H. Seo, J. Cho, J. Han, J. Han, H. Yun, H. Kim, J. Lee, B. Min, J. Yoo and Y. S. Kim, *Small*, 2024, **20**, 9.
9. J. C. Sun, J. Jiang, J. J. He, L. Cao and Q. F. Wang, *Journal of the Electrochemical Society*, 2025, **172**, 7.
10. R. J. Zhou, Z. Y. Gong, X. F. Gui and J. W. Hu, *Appl. Surf. Sci.*, 2025, **706**, 11.
11. Z. Q. Li, D. X. Li, X. F. Sun, Y. X. Xue, Y. H. Shi, Y. L. Fu, C. X. Luo, Q. Lin, X. F. Gui and K. Xu, *J. Energy Storage*, 2024, **93**, 11.
12. L. L. Hu, M. H. Jin, Z. Zhang, H. X. Chen, F. B. Ajdari and J. X. Song, *Advanced Functional Materials*, 2022, **32**, 9.
13. H. Liu, E. Huangzhang, C. Sun, Y. Fan, Z. Ma, X. Zhao and J. Nan, *ACS Omega*, 2021, **6**, 26805-26813.
14. W. Tan, B. Liang, H. Xiao, M. H. Chen, W. J. Yang, X. He, J. H. Hu, K. Zeng and G. Yang, *ACS Appl. Mater. Interfaces*, 2025, **17**, 40375-40387.
15. B. Gendensuren and E. S. Oh, *J. Power Sources*, 2018, **384**, 379-386.
16. C. X. Yang, J. H. Zhang, S. Zhang, Z. Y. Song, D. Y. Li, C. Q. Wang, K. Wang and J. G. Liu, *J. Energy Storage*, 2025, **138**, 10.
17. L. Yang, T. Meng, W. Zheng, J. Zhong, H. Cheng, Y. Tong and D. Shu, *Energy Storage Materials*, 2024, **72**, 103766.
18. E. Feyzi, A. K. M R, X. Li, S. Deng, J. Nanda and K. Zaghib, *Next Energy*, 2024, **5**, 100176.
19. J. Yoon, J. Lee, H. Kim, J. Kim and H. J. Jin, *Polymers*, 2024, **16**, 27.
20. L. I. Jacob and W. Pauer, *Polymers*, 2022, **14**, 14.